Development 139, 3644-3652 (2012) doi:10.1242/dev.082362

Dynamic microtubules at the vegetal cortex predict the embryonic axis in zebrafish

Long Duc Tran[1,2], Hiromu Hino[3,4], Helen Quach[1], Shimin Lim[1,5], Asako Shindo[6], Yuko Mimori-Kiyosue[7], Marina Mione[8], Naoto Ueno[6], Christoph Winkler[2], Masahiko Hibi[3,4,7] and Karuna Sampath[1,2,5,*]

SUMMARY

In zebrafish, as in many animals, maternal dorsal determinants are vegetally localized in the egg and are transported after fertilization in a microtubule-dependent manner. However, the organization of early microtubules, their dynamics and their contribution to axis formation are not fully understood. Using live imaging, we identified two populations of microtubules, perpendicular bundles and parallel arrays, which are directionally oriented and detected exclusively at the vegetal cortex before the first cell division. Perpendicular bundles emanate from the vegetal cortex, extend towards the blastoderm, and orient along the animal-vegetal axis. Parallel arrays become asymmetric on the vegetal cortex, and orient towards dorsal. We show that the orientation of microtubules at 20 minutes post-fertilization can predict where the embryonic dorsal structures in zebrafish will form. Furthermore, we find that parallel microtubule arrays colocalize with *wnt8a* RNA, the candidate maternal dorsal factor. Vegetal cytoplasmic granules are displaced with parallel arrays by ~20°, providing in vivo evidence of a cortical rotation-like process in zebrafish. Cortical displacement requires parallel microtubule arrays, and probably contributes to asymmetric transport of maternal determinants. Formation of parallel arrays depends on Ca^{2+} signaling. Thus, microtubule polarity and organization predicts the zebrafish embryonic axis. In addition, our results suggest that cortical rotation-like processes might be more common in early development than previously thought.

KEY WORDS: Microtubule dynamics, Polarity, Embryonic axes, Dorsoventral patterning, Cortical rotation, *wnt8a* RNA, Zebrafish

INTRODUCTION

In many animals, embryonic axis formation requires polarized transport of maternally deposited factors via the microtubule cytoskeleton. For example, parallel microtubule arrays were shown to be crucial for dorsal axis specification in frog embryos (Elinson and Ninomiya, 2003; Elinson and Rowning, 1988; Rowning et al., 1997). In *Drosophila*, microtubule orientation and polarity determine directional transport of *bicoid* and *oskar* transcripts in oocytes (Brendza et al., 2000; Cha et al., 2001; Glotzer et al., 1997; Pokrywka and Stephenson, 1991; Pokrywka and Stephenson, 1995; Riechmann and Ephrussi, 2001; Schnorrer et al., 2000; Weil et al., 2006; Zimyanin et al., 2008), and *fushi tarazu* and *wingless* transcripts in embryos (Bullock and Ish-Horowicz, 2001; Delanoue and Davis, 2005; Lall et al., 1999; Wilkie and Davis, 2001). Disruption of the microtubule cytoskeleton has severe consequences on oocyte polarity and embryonic patterning in these animals (Elinson and Pasceri, 1989; Lecuyer et al., 2007; Steinhauer and Kalderon, 2006).

In zebrafish embryos, the microtubule cytoskeleton has been shown to have several important functions. Epiboly movements, yolk syncytial layer formation and axonal transport are all processes that require an intact microtubule cytoskeleton (Du et al., 2012; Guzik and Goldstein, 2004; Hsu et al., 2006; Lachnit et al., 2008; Solnica-Krezel and Driever, 1994; Strahle and Jesuthasan, 1993; Takesono et al., 2012). Parallel microtubule arrays in early zebrafish embryos were first described by Jesuthasan and Strahle (Jesuthasan and Strahle, 1997), by Tubulin immunostaining in fixed embryos. However, the dynamics and behavior of these arrays were not investigated further, and the polarity of early microtubule arrays with respect to the embryonic axes was also unknown.

Here, we use transgenic reporters marking the microtubule cytoskeleton and plus-ends of microtubules to investigate microtubule dynamics and polarity in early zebrafish embryos. We show that there are two dynamic microtubule populations in the vegetal cortex that are aligned with or oriented along two of the three embryonic axes. We describe the dynamics and polarity of one of these populations and show that parallel arrays are oriented towards future embryonic dorsal. Thus, the formation and orientation of parallel arrays at 20 minutes post-fertilization (mpf) is the earliest visible marker of future dorsal. Our findings show that microtubules at the vegetal cortex are dynamically remodeled and predict the early embryonic axis in zebrafish.

MATERIALS AND METHODS

Transgenic fish

All experiments were carried out according to the institutional animal care and use guidelines, using standard procedures (Westerfield, 2007). Transgenic zebrafish lines expressing the following microtubule markers were used for live imaging: (1) *Tg(ef1α:dclk-GFP)* transgene contains two doublecortin domains (microtubule-binding domain) of zebrafish *dclk1* fused to *gfp*, and under the control of the *Xenopus ef1α* promoter; (2) *Tg(zpc:Mmu.Eb1-GFP)* fish was generated by injecting a Tol2 plasmid containing a part of *zona pellucida protein C* promoter (Onichtchouk et al.,

[1]Temasek Life Sciences Laboratory, 1 Research Link, 117604 Singapore. [2]Department of Biological Sciences, National University of Singapore, 14 Science Drive 4, 117543 Singapore. [3]Laboratory of Organogenesis and Organ Functions, Bioscience and Biotechnology Center, Nagoya University, Nagoya 464-8601, Japan. [4]Division of Biological Science, Graduate School of Science, Nagoya University, Nagoya 464-8602, Japan. [5]School of Biological Sciences, Nanyang Technological University, 60 Nanyang Drive, 637551 Singapore. [6]National Institute of Basic Biology, Nishigonaka 38, Myodaiji, Okazaki 444-8585 Aichi, Japan. [7]RIKEN Center for Developmental Biology, Kobe 650-0047, Japan. [8]Institute of Toxicology and Genetics, Karlsruhe Institute of Technology, Karlsruhe, Germany.

*Author for correspondence (karuna@tll.org.sg)

Accepted 4 July 2012

2003), and murine EB1-GFP coding sequences (Mimori-Kiyosue et al., 2000), together with *Tol2* transposase mRNA into 1-cell stage embryos (Kawakami et al., 2004); (3) *Tg(Xen.ef1α:Hsa.EB3-GFP)* fish were generated by injecting a Ds plasmid containing the *Xenopus ef1α* promoter (Johnson and Krieg, 1994) and human EB3-GFP sequences (Stepanova et al., 2003), together with *Ac* transposase mRNA into 1-cell stage zebrafish embryos (Emelyanov et al., 2006).

Capped fluorescent RNA synthesis and injections

Fluorescent Alexa 568 UTP-labeled *wnt8a* RNA was synthesized from linearized pCS2+wnt8a:wnt8a UTR plasmid DNA, injected into mature eggs from *Tg(ef1α:dclk-GFP)* females, and fertilized with wild-type sperm (Gilligan et al., 2011; Gore et al., 2005). Fertilized embryos were dechorionated and embedded in 0.7% low melting agarose. RNA localization was examined from 15 mpf onwards, and imaged using a 40× lens with a Numerical Aperture (N.A.) of 1.3 on a custom-built spinning disk system 1 (Nikon Eclipse T*i* microscope fitted to a Yokogawa CSU-X1 confocal scan unit, and a Photometrics CoolSnap HQ^2 camera, controlled by Metamorph 7.7, Molecular Devices).

Live imaging

Transgenic embryos or unfertilized, activated eggs were dechorionated in 30% Danieau's solution, embedded in 0.6-1.1% low melting agarose on a No. 1.5 cover-slip and imaged at the vegetal pole at 28.5°C. To study the structure and dynamics of microtubules, *Tg(ef1α:dclk-GFP)* activated eggs and embryos were imaged using a 100× lens (N.A. 1.4), a 63× lens (N.A. 1.4) or a 40× lens (N.A. 1.3) on a custom-built spinning disk system 2 (Zeiss Axiovert 200M microscope fitted to a Yokogawa CSU21 confocal scan unit, and a Hamamatsu C4742-80-12AG camera, controlled by Metamorph 7.6, Molecular Devices). *z*-stacks were acquired with step sizes of 0.3-0.6 μm at 15- to 90-second intervals, starting at ~0.2 hpf and imaged for ~1 hour.

To examine the orientation of parallel microtubules, *Tg(Xen.ef1α:Hsa.EB3-GFP)* embryos were manually dechorionated, and imaged at a single *z*-plane at 0.8-second intervals on the spinning disk system 2 using a 100× lens (N.A. 1.4). *Tg(zpc:Mmu.Eb1-GFP)* embryos were dechorionated with pronase (1 mg/ml in E3 medium), and imaged at 4-second intervals on a LSM700 confocal microscope (Carl Zeiss) using either a 40× (N.A. 1.3) or a 63× lens (N.A. 1.4). Embryos were kept in agarose and imaged at gastrula stages to identify the position of the shield.

Image processing and data analysis

The three-dimensional (3D) structure of microtubules at the vegetal cortex was rendered by Imaris 7.3 or 7.4 (Bitplane), exported as .tif files, and processed using MBF-ImageJ (http://www.macbiophotonics.ca/imagej/) core 1.46 and the Resize plugin (Munoz et al., 2001). Images in Fig. 1A-D and Fig. 5A-H were 3D deconvoluted by AutoQuant X2.1.3 (Media Cybernetics) using default settings (adaptive PSF, ten iterations, medium noise) and visualized by Imaris. To track cortical granule movement, a two-dimensional (2D) maximum intensity *z*-projection was generated using Metamorph. Cortical granules (apparent as dark spherical areas lacking fluorescent Dclk2-GFP signal in videos) were tracked using MTrackJ plugin (Meijering et al., 2012) in ImageJ 1.46. We tracked 45 cortical granules in five embryos, from ~14 mpf to 40 mpf. Measurement data were exported to a tab-delimited file and analyzed using Microsoft Excel. To study movement of EB1-GFP, 50 comets at ~20 mpf, and 30 comets at ~ 35 mpf, were tracked in each embryo using the Manual Tracking plugin in ImageJ 1.43u. The position of each comet was determined at three consecutive time points, and slope of the track was calculated by the LINEST function in Microsoft Excel. Deviation angles between EB1-GFP tracks and the embryonic shield were calculated, assigned into classes of 10°, ranging from –180° to +180°, and plotted as a histogram.

To examine the correlation between parallel arrays and the dorsal organizer, parallel microtubules at the vegetal cortex of *Tg(ef1α:dclk-GFP)* embryos mounted in 0.9-1.1% low melting agarose were imaged at ~20-40 mpf using a 63× objective lens with N.A. 1.25 on a wide-field Zeiss Axiovert 200M microscope. Embryos were allowed to develop and were imaged during gastrulation to identify the position of the organizer using a 10× objective lens (N.A. 0.3). The deviation angle between parallel arrays and the organizer was measured by drawing a line representing the direction of parallel arrays, and determining its position on the gastrula stage image relative to the embryonic shield, by ROI Manager. The angle between the line and the shield was measured using the 'angle' tool of ImageJ 1.46. Measurements were exported to a tab-delimited file and analyzed using Microsoft Excel. Deviation angles were calculated and assigned into classes of 10°, ranging from –90° to +90° and plotted as a histogram.

Immunostaining

Embryos or unfertilized, activated eggs were fixed and immunostained for α-Tubulin as described (Topczewski and Solnica-Krezel, 1999). Briefly, embryos were dechorionated and fixed in microtubule assembly buffer [80 mM KPIPES (pH 6.5), 5 mM EGTA, 1 mM $MgCl_2$, 3.7% formaldehyde, 0.25% glutaraldehyde, 0.5 μM taxol, and 0.2% Triton X-100] for 6 hours at room temperature (RT). Fixed embryos were dehydrated and kept in methanol at –20°C overnight, rehydrated in phosphate buffered saline (PBS) containing 0.1% NP40, incubated in 100 mM $NaBH_4$ in PBS for 6-16 hours at RT, and washed extensively in tris-buffered saline (TBS). After blocking in TBS containing 2% BSA and 5% normal goat serum for 30 minutes at RT, embryos were incubated with mouse monoclonal antibody against human α-tubulin (Sigma-Aldrich, clone B-5-1-2, 1:400 dilution) at 4°C overnight, washed with five changes of TBS at RT, and incubated with Alexa488-conjugated goat anti-mouse secondary antibody (Invitrogen, 1:4000) for 2-3 hours at RT. Embryos were washed in TBS at 4°C overnight, cleared, and mounted in 100% glycerol for imaging on a Leica SP5 confocal microscope using 100× (N.A. 1.35), 40× (N.A. 1.25) or 20× lenses (N.A. 0.7). To detect nuclear β-Catenin, 256-cell and 1000-cell stage embryos were fixed in 4% paraformaldehyde in PBS and processed for fluorescent immunohistochemistry using a rabbit polyclonal anti-β-Catenin antibody (C2206, Sigma) and Alexa488-conjugated goat anti-rabbit secondary antibodies (Molecular Probes). Images of β-Catenin- and DAPI-stained embryos were acquired using a Zeiss LSM 5 Exciter upright confocal microscope. Approximately 15-25 optical sections at 1.76 μm intervals were examined per embryo. We detected β-Catenin-positive nuclei in many sections. However, owing to intense membrane and cytoplasmic β-Catenin staining that obscured nuclear staining upon *z*-projection of all sections obtained, three serial confocal sections for each embryo were selected, *z*-projected using LSM Image-browser software, and cropped using Adobe Photoshop.

Drug treatments

Unfertilized eggs were activated upon placing in egg water. Activated wild-type eggs and fertilized embryos were incubated in 1 μM thapsigargin (Fermentek) from 5 minutes post-activation (mpa), dechorionated, and fixed at 25 mpa or 25 mpf, respectively. Fixed eggs and embryos were processed for immunostaining with α-Tubulin antibodies to detect parallel arrays. For nocodazole-bead treatments, Affi-Gel blue beads (Bio-Rad) were soaked in 25 μg/ml nocodazole (Sigma-Aldrich) for at least 30 minutes at RT and embedded in agarose, abutting *Tg(ef1α:dclk-GFP)* embryos. Microtubule images were acquired with a 40× lens (N.A. 1.3) on the custom-built spinning disk system 1.

RESULTS

A novel population of microtubules at the vegetal cortex aligning with the animal-vegetal axis

We obtained embryos from *Tg(ef1α:dclk-GFP)* fish and observed microtubule dynamics at the vegetal cortex soon after fertilization. Several bundles of microtubules are observed ~15-30 μm from the cortex (Fig. 1A-D; supplementary material Movie 1). These bundles are perpendicular to the vegetal cortex, and move towards the animal pole. Perpendicular bundles are transient, detected only in the first 10-30 mpf and are not observed subsequently. As perpendicular bundles are oriented along the animal-vegetal axis, they are likely to transport maternal factors, such as *sqt* (*ndr1* – Zebrafish Information Network) RNA (Gore et al., 2005; Gore and Sampath, 2002), through the yolk to the blastoderm. Because these

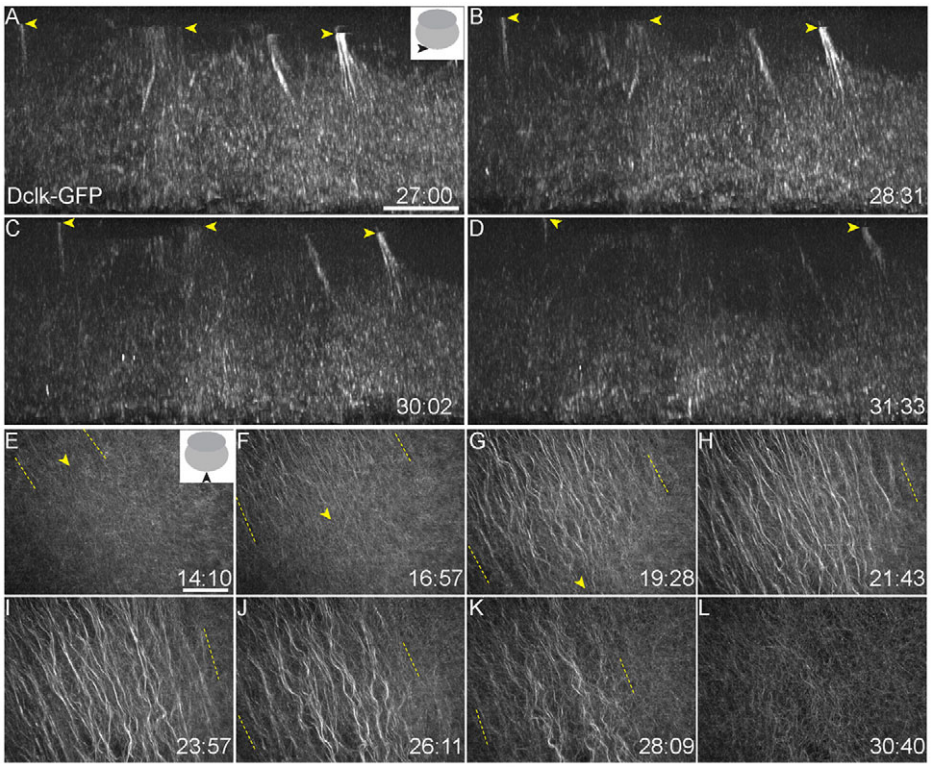

Fig. 1. Microtubule populations at the vegetal cortex of zebrafish embryos. (**A-D**) *Tg(ef1α:dclk-GFP)* expression shows perpendicular bundles at a depth of ~15-30 μm inside the vegetal cortex, oriented along the animal-vegetal axis of the embryo. Yellow arrowheads indicate the position of perpendicular bundles moving through the yolk. (**E-L**) Parallel arrays form from ~14 mpf, grow directionally and extend to cover a large area of the vegetal cortex before dissociating from 26 mpf. Parallel arrays are replaced by a non-directional meshwork (L) by ~30 mpf. Yellow arrowheads (E-G) mark the front and yellow dashed lines (E-K) indicate the spread of parallel arrays. Insets in A and E show schematic of views, and viewing orientation is shown with solid black arrowheads. Numbers at bottom right of panels indicate mpf. Scale bars: in A, 10 μm; in E, 40 μm.

arrays project deep into the yolk, visualizing this population in live embryos is difficult beyond 75-100 μm from the vegetal cortex with current live imaging methodologies. It is not known whether similar perpendicular bundles are present in other chordate embryos.

Concurrently with the perpendicular bundles, we observed a second population of microtubules at the vegetal pole, located more cortically. These are parallel microtubule arrays, which are also transient and dynamic. Parallel arrays grow rapidly from ~15 mpf (Fig. 1E-I), elongate, bundle, and begin to dissociate from ~25 mpf (Fig. 1J,K). Parallel arrays cannot be detected by ~30 mpf (Fig. 1L), and are replaced by a non-directional meshwork of microtubules (supplementary material Movie 2). Thus, both perpendicular and parallel arrays of microtubules are transiently detected at the vegetal cortex and are observed only within the first 30 mpf.

Parallel arrays become asymmetric, and their orientation corresponds with embryonic dorsal

Immunostaining using antibodies to detect α-Tubulin shows that parallel microtubule arrays become asymmetric (Fig. 2A,B) with respect to the vegetal pole of the embryo. Parallel arrays span a region encompassing a ~45° sector of the embryo and extend nearly a third of the distance from the vegetal pole towards the animal pole of the embryo. Thus, parallel microtubule arrays cover an extensive region of the early embryo, and we found their spread to be similar to the expression domain of asymmetrically localized maternal *wnt8a* transcripts (Fig. 2C; supplementary material Fig. S1) in early embryos (Lu et al., 2011). Therefore, we investigated whether *wnt8a* RNA colocalizes with the parallel arrays. Alexa568 UTP-labeled fluorescent *wnt8a* RNA was injected into eggs from *Tg(ef1α:dclk-GFP)* females, which were then fertilized and observed at the vegetal pole. Punctate aggregates of fluorescent *wnt8a* RNA can be detected localizing with the Dclk2-GFP-marked parallel arrays by ~20 mpf (Fig. 2D; *n*=6 embryos), and by 35 mpf, similar to endogenous *wnt8a* RNA, injected fluorescent RNA is detected asymmetrically on the vegetal lateral cortex and in the blastoderm (Fig. 2I). Furthermore, fluorescent *wnt8a* punctae are not observed outside of the region covered by the parallel arrays (see bottom left area of Fig. 2D). Thus, *wnt8a* RNA colocalizes with parallel microtubule arrays.

To determine whether the asymmetric localization of the parallel arrays corresponds to the embryonic axes, we observed the arrays as they formed in real time in agarose-embedded *Tg(ef1α:dclk-GFP)* embryos, and marked the orientation along which parallel arrays were aligned (Fig. 2F,H, blue line). We later marked where the dorsal organizer, the shield (Fig. 2G,H, red arrow), formed in each embryo during gastrulation and determined the difference in angle (δ) between orientation of the parallel arrays in early embryos and the position of the shield (Fig. 2H). In most embryos (>90%, *n*=23), the shield forms within 30° of the orientation of parallel arrays (Fig. 2K). Thus, orientation of parallel arrays corresponds to future embryonic dorsal.

Plus ends of parallel arrays are oriented towards dorsal

To determine the directionality of parallel arrays, we used two transgenic lines labeling the growing ('plus') ends of microtubules, *Tg(zpc:Mmu.Eb1-GFP)* and *Tg(Xen.ef1α:Hsa.EB3-GFP)*, and observed the growing tips of microtubules by live imaging (supplementary material Movies 3-6). Comets of EB1-GFP plus-ends were tracked over time and the direction of the plus-ends versus the position of the dorsal shield at gastrula stages was determined (Fig. 2E,J). Within the first 30 mpf, most plus-ends are oriented directionally, towards future embryonic dorsal (Fig. 2L). The angle of deviation (δ), between the direction of plus-ends and the shield, is <20° for >80% of the tracks (Fig. 2L; supplementary

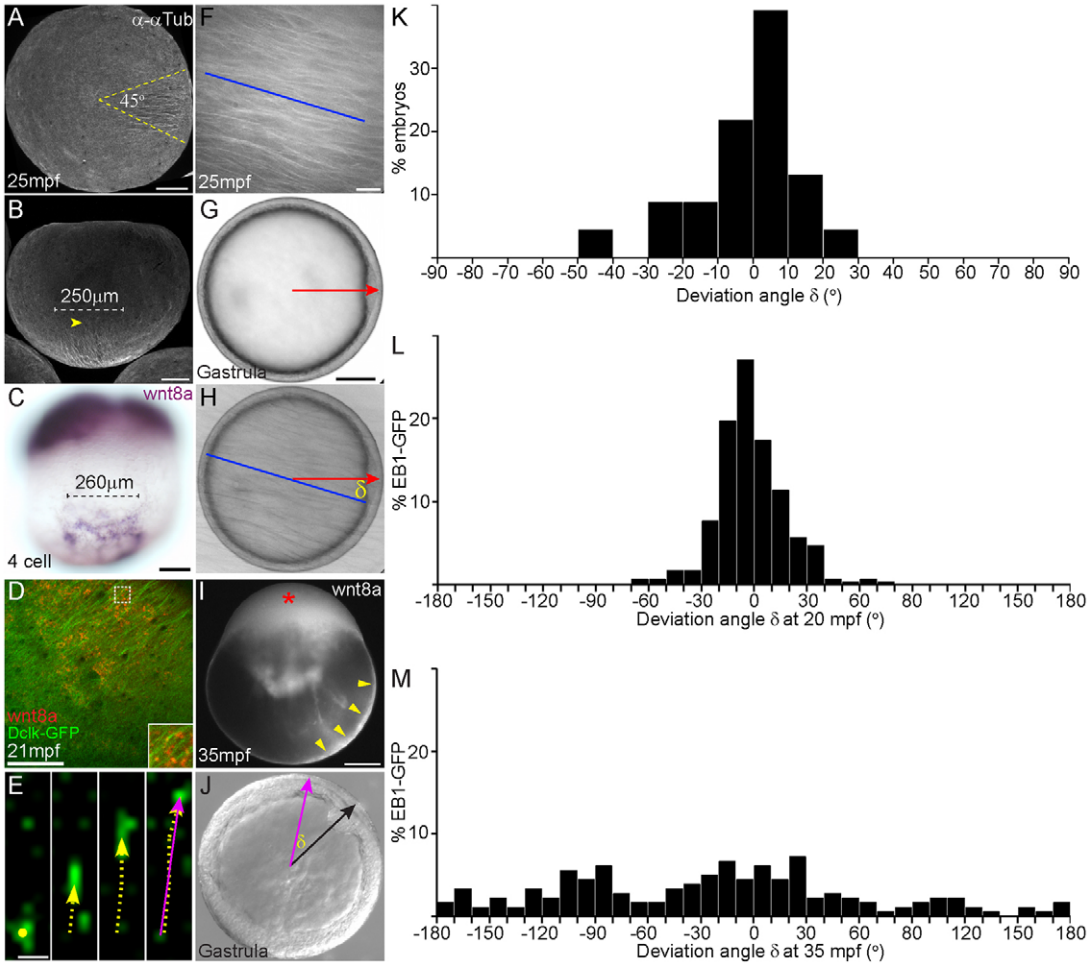

Fig. 2. Parallel microtubule arrays are directed towards embryonic dorsal. (**A**,**B**) Immunostaining to detect α-Tubulin shows that parallel arrays form asymmetrically at one side of the vegetal cortex and cover a sector of ~45°. Yellow dashed lines in A mark the extent of spread; yellow arrowhead in B marks one end of parallel arrays. (**C**) Parallel arrays are spread over ~250 μm, similar to the spread of *wnt8a* transcripts at early cleavage stages. (**D**) Colocalization of parallel arrays (Dclk2-GFP in green) and fluorescent injected Alexa568 UTP-labeled *wnt8a* RNA (red punctae) at ~20 mpf is shown. Inset shows higher magnification of area marked with white dotted square. (**E-M**) Injected fluorescent *wnt8a* RNA localizes asymmetrically to the vegetal lateral cortex (yellow arrowheads in I) and to the blastoderm (red asterisk in I), similar to endogenous *wnt8a* transcripts. (F-M) Orientation of parallel arrays at 20-30 mpf (F), compared with position of the dorsal organizer (shield, red arrow in G,H) at gastrulation (G), and the difference between orientation of parallel arrays and the position of the shield was used to calculate the deviation angle (δ) (H). More than 90% of embryos formed the shield within 30° of the parallel arrays (K) (*n*=23 embryos). EB1-GFP comets were tracked at 4-second intervals (E), starting at 20 mpf (L) or 35 mpf (M). Direction of movement of each comet was calculated and is presented as a purple arrow (E,J). 50 comets were tracked at 20 mpf and 30 comets at 35 mpf, *n*=6 embryos. The position of the shield was identified during gastrulation (black arrow in J), and the angle of deviation (δ) was calculated. Graph in L shows that most comets moved towards the future dorsal organizer at 20 mpf, whereas at 35 mpf (graph in M), comets at the same location moved randomly. A,D-H,J vegetal views; B,C,I, lateral views. Scale bars: in A-C,G,I, 100 μm; in D, 50 μm; in E, 1 μm; in F, 10 μm.

material Movie 3). However, after 30 mpf, when parallel arrays dissociate, EB1-GFP comets move in all directions and the deviation angle shows a range (Fig. 2M; supplementary material Movie 4). Similar findings were obtained using embryos expressing a different plus-end binding protein, EB3-GFP (supplementary material Movies 5, 6). We tracked the speed of the comets and find that the average EB3-GFP particle speed before 30 mpf (when parallel arrays are present and comets move directionally), is 0.38 μm/second (*n*=40 comets), and this increases to 0.62 μm/second (*n*=30 comets) when the EB3-GFP comets move in all directions. Therefore, the plus-ends of parallel arrays at the vegetal cortex of zebrafish embryos are oriented towards future embryonic dorsal.

Cortical granules move along parallel arrays

We observed several dense cytoplasmic granules (Fig. 3A, dotted circles) at the vegetal cortex, which appear to move within the first 30 mpf when parallel arrays are present (supplementary material Movie 7). By tracking individual granules in a time course (Fig. 3A-C, numbered granules), we find that they move rapidly and directionally initially (0.17 μm/second, *n*=29 granules at ~20 mpf; Fig. 3D, Phase 1), and after 30 mpf, the granules slow down (0.02 μm/second, *n*=38 granules at 35 mpf; Fig. 3D, Phase 2), and their movement, if any, is random (supplementary material Fig. S2). Phase 1 correlates with the presence of parallel arrays, and in Phase 2, parallel arrays disappear, giving way to a dense non-directional microtubule meshwork. We find that individual granules move >70

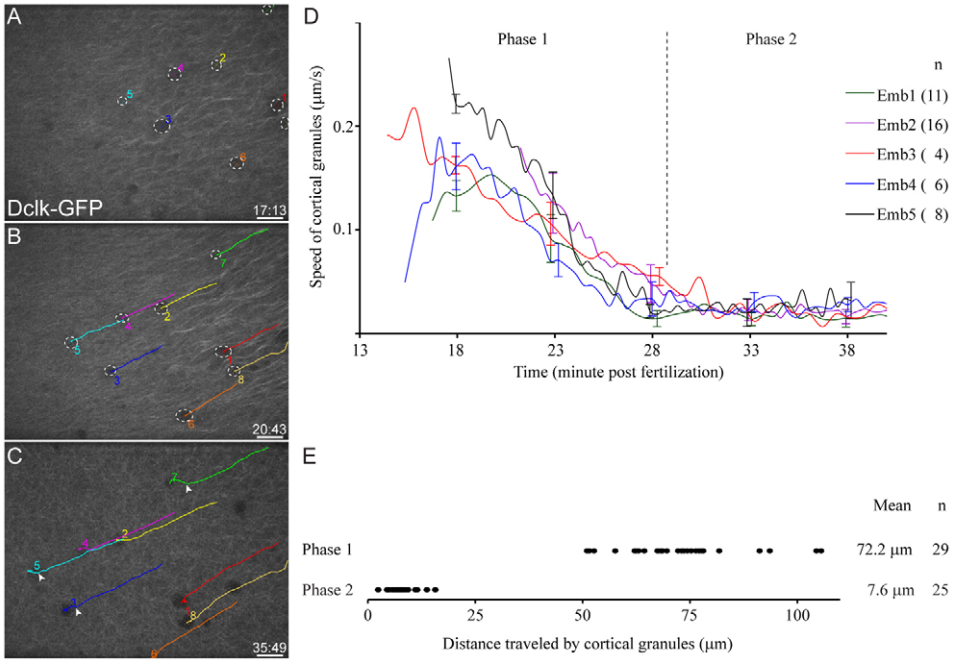

Fig. 3. Cortical granules at the vegetal pole are displaced by 20°. (**A-D**) Cortical granules (dotted white circles in A,B) at the vegetal pole move fast and in the same direction as parallel arrays before 30 mpf (Phase 1; B,D), and move slowly and randomly after parallel arrays disappear (Phase 2; C,D). Colored lines in B and C indicate individual cortical granules that were numbered and tracked. White arrowheads in C mark the position where cortical granules are no longer directional and begin moving randomly. (**D**) Each line shows the average speed of cortical granules in each embryo (number of granules tracked for each embryo shown in parentheses). Error bars are shown for selected time points and represent s.d. (**E**) Graph shows the distance traveled by individual cortical granules, and this measurement was used to calculate the angle of displacement. The cortical granules are displaced by ~20°. Scale bars: 20 μm.

μm in Phase I, and some granules move up to 110 μm, whereas in Phase 2, the granules typically move <8 μm (Fig. 3E) and their movement is non-directional. The distance of 70-100 μm traveled by granules along parallel arrays at the vegetal cortex (in embryos with a diameter of ~500 μm) corresponds to a ~20° displacement of the granules along the cortex. These results suggest that vegetal cytoplasmic granules in zebrafish embryos undergo a cortical rotation-like shift, similar to that observed in early *Xenopus* embryos.

To determine whether granule movement is dependent on parallel microtubule arrays, we transiently disrupted microtubules in a small region of the cortex by local application of a bead soaked in nocodazole (Fig. 4A-D, schematic). The extent of disruption of microtubules in bead-treated embryos was determined by examining the Dclk2-GFP parallel arrays (Fig. 4E-H). We tracked the movement of individual granules in bead-implanted embryos (Fig. 4E-H, yellow asterisks). Granules in embryos treated with control DMSO beads move rapidly and directionally, and their net displacement is at least 82 μm (mean 99 μm; n=8 granules from two embryos; Fig. 4A,E,I,M,S; supplementary material Movie 8). Granules in close proximity to nocodazole beads (Fig. 4B,D) do not move directionally (Fig. 4J,L,N,P; supplementary material Movies 9, 10), exhibit sudden changes in direction (see granule trajectories in Fig. 4N), and the net distance traveled is also reduced to ~25 μm (n=24 granules from two embryos; Fig. 4S). Granules located further from nocodazole beads (Fig. 4C) move directionally (Fig. 4K,O; supplementary material Movie 10) together with parallel arrays that are visible (Fig. 4G). Thus, directional movement of vegetal cortical granules is dependent on parallel microtubule arrays.

To determine how the dorsoventral axis is affected by transient nocodazole-bead treatment and parallel array disruption, we examined the nuclear accumulation of the early dorsal marker β-Catenin. In DMSO-bead treated embryos, in which normal parallel arrays formed (supplementary material Fig. S3A), we detected β-Catenin in many dorsal nuclei (Fig. 4Q; supplementary material Fig. S3B-D) whereas in nocodazole-bead treated embryos with disrupted parallel arrays (supplementary material Fig. S3E), we did not detect any nuclear β-Catenin accumulation (Fig. 4R; supplementary material Fig. S3F-H). Therefore, local disruption of parallel microtubule arrays affects the directional transport of vegetal cytoplasmic granules and disrupts specification of the dorsal axis.

Formation of parallel arrays is independent of sperm entry and fertilization

The vegetal cortex of zebrafish embryos has dense cytoplasmic granules that appear to undergo cortical rotation-like movement similar to that observed in *Xenopus* embryos. In *Xenopus*, it is thought that sperm entry and fertilization trigger movement of the cortex (Gerhart et al., 1989; Gerhart et al., 1981; Vincent et al., 1986), which then shifts by 30° relative to the point of sperm entry (Vincent et al., 1986). However, in zebrafish, the sperm entry point is fixed, and is a defined channel in the chorionic membrane, the micropyle, located at the animal pole of the egg (Hart and Donovan, 1983). So, we tested whether fertilization is even necessary for formation of parallel arrays. We artificially activated squeezed mature eggs and examined microtubule dynamics at the vegetal cortex. Remarkably, parallel arrays form in unfertilized, activated zebrafish eggs at ~20 mpf (Fig. 5A-H; supplementary material Movie 11). Parallel microtubule arrays in unfertilized, activated eggs become elongated and dense, and, similar to arrays in fertilized embryos, they dissociate by 34 mpf. Thus, parallel arrays form independently of sperm entry and fertilization.

Formation of parallel arrays is dependent on Ca^{2+} transients

So what might trigger parallel array formation? Waves of Ca^{2+} transients have been observed in early zebrafish eggs (Lee et al., 1999; Leung et al., 1998), and disruption of Ca^{2+} signaling is thought to affect embryonic dorsoventral patterning (Westfall et al., 2003). Therefore, we tested whether Ca^{2+} signaling is required for parallel array formation. Activated unfertilized eggs were treated with the drug thapsigargin, which inhibits intracellular Ca^{2+} pumps, and formation of arrays was observed in treated eggs. Unactivated

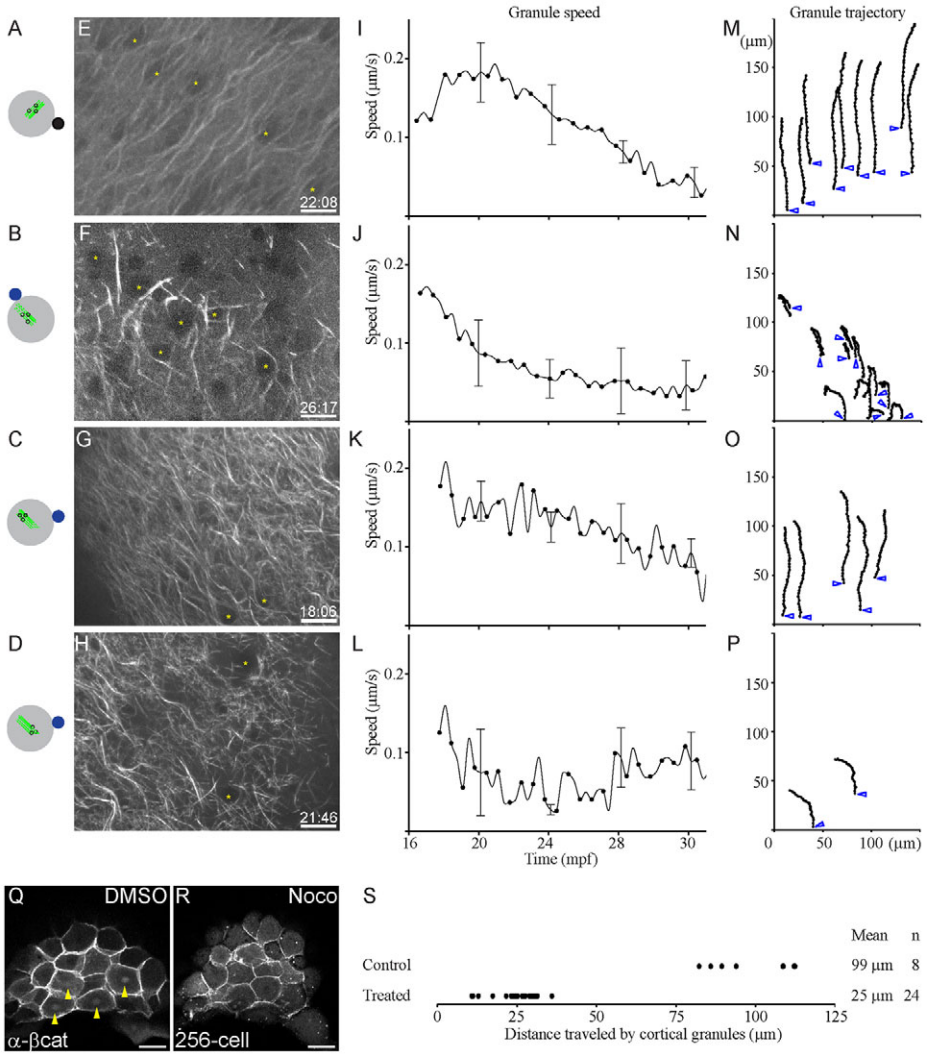

Fig. 4. Directional movement of vegetal cortical granules is dependent on parallel microtubule arrays. (**A-D**) Schematics showing position of beads relative to the arrays. DMSO bead is shown as a solid black circle (A); nocodazole beads are shown as solid blue circles (B-D); parallel arrays are shown as solid green lines (A-D), nocodazole-disrupted arrays as dashed green lines (B-D), and granules are depicted as open black circles (A-D). (**E-H**) Dclk2-GFP-labeled arrays show extent of disruption of microtubules in bead-treated embryos (time of image in mpf at bottom right of each panel; yellow asterisks indicate granules tracked). (**I-L**) Granules in embryos treated with DMSO control beads and granules at a distance from nocodazole-soaked beads travel faster (A,C,I,K), than granules adjacent to nocodazole beads (B,D,J,L), which do not show much movement. Graphs in K,L are from granules at different locations in the same embryo. (**M-P**) Tracking the trajectory of the granules shows that DMSO control beads do not affect directed granule movement (M), similar to granules at a distance from nocodazole-soaked beads (O). By contrast, granules near nocodazole-soaked beads show random movement, and sudden changes in the direction of movement (N,P). Trajectory of individual granules is shown as hatched black lines; blue open arrowheads show initial granule position. (**Q**,**R**) Absence of nuclear β-Catenin accumulation in dorsal cells (R) indicates the effect of transient and local nocodazole treatment on dorsal specification in comparison to control DMSO treatment (Q; yellow arrowheads indicate β-Catenin-positive nuclei). (**S**) Distance traveled by individual cortical granules in control bead or nocodazole bead-treated embryos. Scale bars: in E-H, 15 μm; in Q,R, 50 μm.

eggs do not show any parallel arrays (Fig. 5I). In contrast to control DMSO-treated eggs (n=27; Fig. 5J,O), thapsigargin-treated eggs either show reduced/abnormal bundles (16%, n=44; Fig. 5K,O) or no parallel arrays at all (84%, n=44; Fig. 5L,O). Therefore, formation of parallel arrays depends on Ca^{2+} signaling.

Ca^{2+} signaling has been shown to be a trigger for cortical granule exocytosis in zebrafish. The cortical microtubule network in maternal *brom bones*/*hnRNP1* mutant embryos, which are defective in dorsoventral patterning, is disorganized, presumably owing to failure of granule exocytosis, and can be rescued by providing Ca^{2+} (Mei et al., 2009; Wagner et al., 2004). Thus, in our drug-treated embryos, and in the Westfall et al. experiments (Westfall et al., 2003), the reduced/abnormal parallel arrays caused by Ca^{2+} inhibition probably lead to dorsoventral defects. To test this, we examined nuclear accumulation of β-Catenin in dorsal cells of thapsigargin-treated embryos. We find that in comparison to control DMSO-treated embryos, which show numerous β-Catenin-positive nuclei (Fig. 5M; supplementary material Fig. S4A-C), there were no detectable β-Catenin-positive nuclei in thapsigargin-treated embryos (Fig. 5N; supplementary material Fig. S4D-F). Thus, disruption of parallel arrays by interfering with Ca^{2+} signaling leads to disruption of dorsal axis formation.

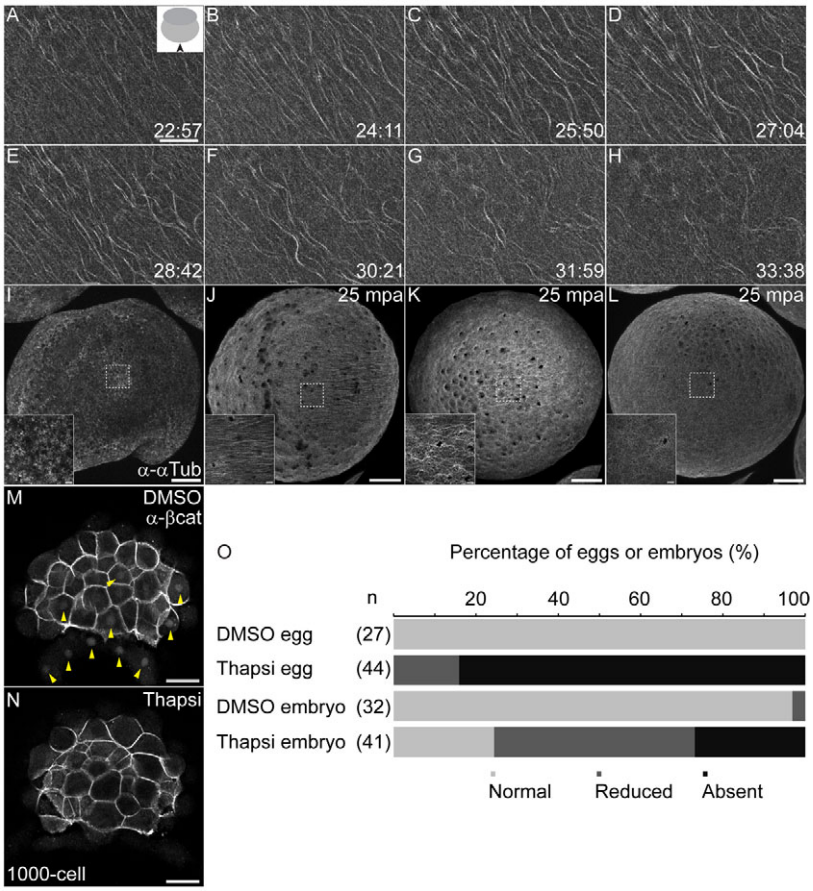

Fig. 5. Formation of parallel arrays is independent of fertilization but dependent on calcium signaling. (**A-H**) Parallel arrays form in unfertilized, activated eggs, and show similar dynamics to arrays in fertilized embryos. Inset in A shows schematic of view, and viewing direction is shown with a solid black arrowhead. (**I-L**) Parallel arrays are not detected in unactivated eggs (I), in comparison with normal arrays (J) observed in DMSO-treated and reduced (K) or missing (L) arrays in thapsigargin-treated, unfertilized eggs. Insets in I-L show magnified images of regions marked by white dashed squares. (**M**,**N**) Thapsigargin-treated embryos show loss of nuclear β-Catenin (N) in comparison with control DMSO-treated embryos (M, yellow arrowheads indicate β-Catenin-positive nuclei in the yolk syncytial layer and blastoderm). (**O**) Percentage of eggs or embryos with absent (black), reduced (dark gray) or normal (pale gray) parallel arrays from DMSO or thapsigargin-treatments. Number of eggs/embryos are indicted in parentheses. Scale bars: in A, 20 μm; in I-L, 100 μm; in I-L insets, 10 μm; in M,N, 50 μm.

DISCUSSION

Our results show that parallel arrays form autonomously even in activated eggs. This had been suggested from observations of sub-cortical arrays in activated frog eggs (Elinson and Rowning, 1988) and in vegetal fragments of amphibian embryos (Elinson and Palecek, 1993), and it has been suggested that the sperm aster only biases the direction of parallel arrays rather than triggers formation of parallel arrays (Gerhart, 2004). However, as the explants/fragments involved surgical manipulations that have the potential to change intracellular Ca^{2+} fluxes and microtubule polymerization, and thereby indirectly affect microtubule dynamics, it was not entirely clear whether sperm entry and fertilization were necessary for parallel array formation in this organism (Houliston and Elinson, 1991). Thus, our in vivo finding that formation of parallel arrays in zebrafish is independent of sperm entry and fertilization resolves this long-standing question. Our findings are also consistent with the observation that haploid zebrafish embryos still have a normal dorsal axis (Streisinger et al., 1981).

EB1-GFP and EB3-GFP comet movement shows that parallel microtubule arrays are oriented with their plus-ends towards dorsal. Thus, parallel microtubules can directionally transport dorsal determinants from the vegetal pole. These include maternal *wnt8a* RNA, as we have shown, and it is likely that the maternal linker/adapter protein Syntabulin is also transported along parallel microtubule arrays (Lu et al., 2011; Nojima et al., 2010). It is also possible that Wnt8a protein is transported. In *Xenopus*, vesicle-like organelles are enriched in future dorsal cells after cortical rotation, and a Dsh-GFP fusion protein associates with the vesicle-like structures (Miller et al., 1999). GBP-GFP and KLC-GFP particles also exhibit directed translocation during cortical rotation (Weaver et al., 2003). In zebrafish, we observed directional movement of cortical granules along parallel microtubule arrays. It is possible that the transported cortical granules contain components of the Wnt pathway.

This also raises the question of how general cortical rotation-like processes are. There is evidence for a rotation-like activity in actinopterygii and acipenserids, including sturgeons (Abraham et al., 1995; Dettlaff, 1962). Hence, this process has been previously observed in animals other than *Xenopus* and *Rana* (Elinson and Rowning, 1988; Gerhart et al., 1989; Houliston and Elinson, 1991). A rotation-like process has been suggested in lampreys as well (Clavert, 1962). Although it has been reported that eggs of the teleost Medaka do not manifest cortical rotation (Abraham et al., 1995), our results suggest that an apparently similar movement takes place in zebrafish. The expression patterns of maternal *wnt8a* RNA and Syntabulin (also known as Tokkaebi) protein in early zebrafish embryos (Lu et al., 2011; Nojima et al., 2010) also support such a movement. Although we did not find any direct evidence for movement of the cortex per se, asymmetry of the parallel arrays and the directional movement of the vegetal yolk cytoplasm that accompanies it might underlie the transport and displacement of various maternal factors towards future embryonic dorsal in zebrafish.

We find that parallel microtubule arrays are spread over an extensive area spanning ~250 μm in the yolk cell vegetal region. Maternal *wnt8a* transcripts, which we find colocalizing with the parallel arrays, are also distributed over a fairly broad domain of ~250 μm (Fig. 2C). Therefore, the maternal Wnt8 signal from the yolk, which is likely to be diffusible, can potentially access at least

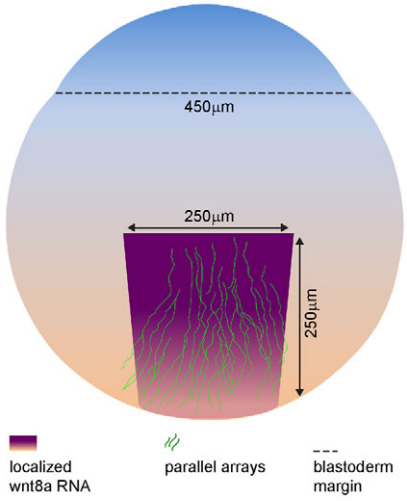

Fig. 6. Schematic of location and extent of parallel arrays compared with maternal *wnt8a* transcript expression in the early zebrafish embryo. An embryo at the 1-cell stage, with the extent of parallel arrays (green lines), *wnt8a* RNA expression (purple), and blastoderm margin (black dashed line) indicated. Expression of *wnt8a* RNA spans nearly one-fifth to one-sixth of the blastoderm margin. Representative 1-cell embryos immunostained for Tubulin were used to trace the parallel arrays and embryo outline.

one-fifth to one-sixth of the blastoderm margin (Fig. 6). Additionally, there is also *wnt8a* expression in the blastoderm (Lu et al., 2011). However, β-Catenin accumulates in the nuclei of a very small number of dorsal cells ((Dougan et al., 2003; Lim et al., 2012). Based on antisense knockdown experiments, Sfrp1a and Frzb were suggested as the factors that negatively regulate Wnt8 activity in the blastoderm to restrict β-Catenin accumulation (Lu et al., 2011). The expression pattern of maternal *sfrp1a* and *frzb* transcripts is not spatially restricted (B. Thisse and C. Thisse, personal communication), and zygotic *sfrp1* and *frzb* RNA are enriched later in dorsal cells (Peng and Westerfield, 2006; Tendeng and Houart, 2006). These transcripts encode secreted Wnt antagonists, which should be freely diffusible as well (Lee et al., 2006; Lin et al., 1997; Mii and Taira, 2009; Pera and De Robertis, 2000; Ploper et al., 2011; Wang et al., 1997). Therefore, it is not clear whether the uniform, maternal Sfrp1a and Frzb activity is sufficient to restrict the response of the broad, maternally expressed dorsal Wnt signal to a few marginal cells. It is possible that additional factors and mechanisms function to limit the range of maternal Wnt activity and to spatially restrict nuclear β-Catenin accumulation to dorsal cells. Identification of these factors will help clarify how maternal *wnt8a*, transported by the vegetal microtubule parallel arrays, is regulated to form future dorsal structures.

Acknowledgements
We thank members of the Hibi laboratory, Sampath laboratory, the Singapore fish community, Mohan Balasubramanian, Claire Canning, Meredith Calvert, Mithilesh Mishra, and Shijie Tao for discussions and suggestions; Hideaki Nojima for generating the Eb1-gfp transgenic line; the TLL sequencing, imaging and fish facilities and the NUS CBIS facility.

Funding
L.D.T. was supported by a Department of Biological Sciences National University of Singapore Graduate research scholarship and Temasek Life Sciences Laboratory. S.L. was supported by a pre-doctoral fellowship from the Singapore Millennium Foundation and Temasek Life Sciences Laboratory. L.D.T. acknowledges an Asia-Pacific Developmental Biology Network travel award to visit N.U.'s laboratory at early stages of this work. Work in the laboratory of M.H. is supported by Grants-in-Aid for Scientific Research from the Ministry of Education, Science, Sports and Technology, Japan [21370103]. Work in the laboratory of K.S. is supported by Temasek Life Sciences Laboratory.

Competing interests statement
The authors declare no competing financial interests.

Supplementary material
Supplementary material available online at
http://dev.biologists.org/lookup/suppl/doi:10.1242/dev.082362/-/DC1

References

Abraham, V. C., Miller, A. L. and Fluck, R. A. (1995). Microtubule arrays during ooplasmic segregation in the medaka fish egg (Oryzias latipes). *Biol. Bull.* **188**, 136-145.
Brendza, R. P., Serbus, L. R., Duffy, J. B. and Saxton, W. M. (2000). A function for kinesin I in the posterior transport of oskar mRNA and Staufen protein. *Science* **289**, 2120-2122.
Bullock, S. L. and Ish-Horowicz, D. (2001). Conserved signals and machinery for RNA transport in Drosophila oogenesis and embryogenesis. *Nature* **414**, 611-616.
Cha, B. J., Koppetsch, B. S. and Theurkauf, W. E. (2001). In vivo analysis of Drosophila bicoid mRNA localization reveals a novel microtubule-dependent axis specification pathway. *Cell* **106**, 35-46.
Clavert, J. (1962). Symmetrization of the egg of vertebrates. *Adv. Morphol.* **2**, 27-60.
Delanoue, R. and Davis, I. (2005). Dynein anchors its mRNA cargo after apical transport in the Drosophila blastoderm embryo. *Cell* **122**, 97-106.
Dettlaff, T. A. (1962). Cortical changes in acipenserid eggs during fertilization and artificial activation. *J. Embryol. Exp. Morphol.* **10**, 1-26.
Dougan, S. T., Warga, R. M., Kane, D. A., Schier, A. F. and Talbot, W. S. (2003). The role of the zebrafish nodal-related genes squint and cyclops in patterning of mesendoderm. *Development* **130**, 1837-1851.
Du, S., Draper, B. W., Mione, M., Moens, C. B. and Bruce, A. (2012). Differential regulation of epiboly initiation and progression by zebrafish Eomesodermin A. *Dev. Biol.* **362**, 11-23.
Elinson, R. P. and Rowning, B. (1988). A transient array of parallel microtubules in frog eggs: potential tracks for a cytoplasmic rotation that specifies the dorso-ventral axis. *Dev. Biol.* **128**, 185-197.
Elinson, R. P. and Pasceri, P. (1989). Two UV-sensitive targets in dorsoanterior specification of frog embryos. *Development* **106**, 511-518.
Elinson, R. P. and Palecek, J. (1993). Independence of two microtubule systems in fertilized frog eggs: the sperm aster and the vegetal parallel array. *Dev. Genes Evol.* **202**, 224-232.
Elinson, R. P. and Ninomiya, H. (2003). Parallel microtubules and other conserved elements of dorsal axial specification in the direct developing frog, Eleutherodactylus coqui. *Dev. Genes Evol.* **213**, 28-34.
Emelyanov, A., Gao, Y., Naqvi, N. I. and Parinov, S. (2006). Trans-kingdom transposition of the maize dissociation element. *Genetics* **174**, 1095-1104.
Gerhart, J. (2004). Symmetry breaking in the egg of xenopus. In *Gastrulation: From Cells to Embryos* (ed. C. D. Stern), pp. 341-351. Cold Spring Harbor, New York: Cold Spring Harbor Laboratory Press.
Gerhart, J., Ubbels, G., Black, S., Hara, K. and Kirschner, M. (1981). A reinvestigation of the role of the grey crescent in axis formation in Senopus laevis. *Nature* **292**, 511-516.
Gerhart, J., Danilchik, M., Doniach, T., Roberts, S., Rowning, B. and Stewart, R. (1989). Cortical rotation of the Xenopus egg: consequences for the anteroposterior pattern of embryonic dorsal development. *Development* **107 Suppl.**, 37-51.
Gilligan, P. C., Kumari, P., Lim, S., Cheong, A., Chang, A. and Sampath, K. (2011). Conservation defines functional motifs in the squint/nodal-related 1 RNA dorsal localization element. *Nucleic Acids Res.* **39**, 3340-3349.
Glotzer, J. B., Saffrich, R., Glotzer, M. and Ephrussi, A. (1997). Cytoplasmic flows localize injected oskar RNA in Drosophila oocytes. *Curr. Biol.* **7**, 326-337.
Gore, A. V. and Sampath, K. (2002). Localization of transcripts of the zebrafish morphogen Squint is dependent on egg activation and the microtubule cytoskeleton. *Mech. Dev.* **112**, 153-156.
Gore, A. V., Maegawa, S., Cheong, A., Gilligan, P. C., Weinberg, E. S. and Sampath, K. (2005). The zebrafish dorsal axis is apparent at the four-cell stage. *Nature* **438**, 1030-1035.
Guzik, B. W. and Goldstein, L. S. (2004). Microtubule-dependent transport in neurons: steps towards an understanding of regulation, function and dysfunction. *Curr. Opin. Cell Biol.* **16**, 443-450.
Hart, N. H. and Donovan, M. (1983). Fine-structure of the chorion and site of sperm entry in the egg of Brachydanio. *J. Exp. Zool.* **227**, 277-296.
Houliston, E. and Elinson, R. P. (1991). Patterns of microtubule polymerization relating to cortical rotation in Xenopus laevis eggs. *Development* **112**, 107-117.

Hsu, H. J., Liang, M. R., Chen, C. T. and Chung, B. C. (2006). Pregnenolone stabilizes microtubules and promotes zebrafish embryonic cell movement. *Nature* **439**, 480-483.
Jesuthasan, S. and Strahle, U. (1997). Dynamic microtubules and specification of the zebrafish embryonic axis. *Curr. Biol.* **7**, 31-42.
Johnson, A. D. and Krieg, P. A. (1994). Pxex, a vector for efficient expression of cloned sequences in xenopus embryos. *Gene* **147**, 223-226.
Kawakami, K., Takeda, H., Kawakami, N., Kobayashi, M., Matsuda, N. and Mishina, M. (2004). A transposon-mediated gene trap approach identifies developmentally regulated genes in zebrafish. *Dev. Cell* **7**, 133-144.
Lachnit, M., Kur, E. and Driever, W. (2008). Alterations of the cytoskeleton in all three embryonic lineages contribute to the epiboly defect of Pou5f1/Oct4 deficient MZspg zebrafish embryos. *Dev. Biol.* **315**, 1-17.
Lall, S., Francis-Lang, H., Flament, A., Norvell, A., Schupbach, T. and Ish-Horowicz, D. (1999). Squid hnRNP protein promotes apical cytoplasmic transport and localization of Drosophila pair-rule transcripts. *Cell* **98**, 171-180.
Lecuyer, E., Yoshida, H., Parthasarathy, N., Alm, C., Babak, T., Cerovina, T., Hughes, T. R., Tomancak, P. and Krause, H. M. (2007). Global analysis of mRNA localization reveals a prominent role in organizing cellular architecture and function. *Cell* **131**, 174-187.
Lee, H. X., Ambrosio, A. L., Reversade, B. and De Robertis, E. M. (2006). Embryonic dorsal-ventral signaling: secreted frizzled-related proteins as inhibitors of tolloid proteinases. *Cell* **124**, 147-159.
Lee, K. W., Webb, S. E. and Miller, A. L. (1999). A wave of free cytosolic calcium traverses zebrafish eggs on activation. *Dev. Biol.* **214**, 168-180.
Leung, C. F., Webb, S. E. and Miller, A. L. (1998). Calcium transients accompany ooplasmic segregation in zebrafish embryos. *Dev. Growth Differ.* **40**, 313-326.
Lim, S., Kumari, P., Gilligan, P., Quach, H. N., Mathavan, S. and Sampath, K. (2012). Dorsal activity of maternal squint is mediated by a non-coding function of the RNA. *Development* **139**, 2903-2915.
Lin, K., Wang, S., Julius, M. A., Kitajewski, J., Moos, M., Jr and Luyten, F. P. (1997). The cysteine-rich frizzled domain of Frzb-1 is required and sufficient for modulation of Wnt signaling. *Proc. Natl. Acad. Sci. USA* **94**, 11196-11200.
Lu, F. I., Thisse, C. and Thisse, B. (2011). Identification and mechanism of regulation of the zebrafish dorsal determinant. *Proc. Natl. Acad. Sci. USA* **108**, 15876-15880.
Mei, W., Lee, K. W., Marlow, F. L., Miller, A. L. and Mullins, M. C. (2009). hnRNP I is required to generate the Ca2+ signal that causes egg activation in zebrafish. *Development* **136**, 3007-3017.
Meijering, E., Dzyubachyk, O. and Smal, I. (2012). Methods for cell and particle tracking. *Methods Enzymol.* **504**, 183-200.
Mii, Y. and Taira, M. (2009). Secreted Frizzled-related proteins enhance the diffusion of Wnt ligands and expand their signalling range. *Development* **136**, 4083-4088.
Miller, J. R., Rowning, B. A., Larabell, C. A., Yang-Snyder, J. A., Bates, R. L. and Moon, R. T. (1999). Establishment of the dorsal-ventral axis in Xenopus embryos coincides with the dorsal enrichment of dishevelled that is dependent on cortical rotation. *J. Cell Biol.* **146**, 427-437.
Mimori-Kiyosue, Y., Shiina, N. and Tsukita, S. (2000). The dynamic behavior of the APC-binding protein EB1 on the distal ends of microtubules. *Curr. Biol.* **10**, 865-868.
Munoz, A., Blu, T. and Unser, M. (2001). Least-squares image resizing using finite differences. *IEEE Trans. Image Process* **10**, 1365-1378.
Nojima, H., Rothhamel, S., Shimizu, T., Kim, C. H., Yonemura, S., Marlow, F. L. and Hibi, M. (2010). Syntabulin, a motor protein linker, controls dorsal determination. *Development* **137**, 923-933.
Onichtchouk, D., Aduroja, K., Belting, H. G., Gnugge, L. and Driever, W. (2003). Transgene driving GFP expression from the promoter of the zona pellucida gene zpc is expressed in oocytes and provides an early marker for gonad differentiation in zebrafish. *Dev. Dyn.* **228**, 393-404.
Peng, G. and Westerfield, M. (2006). Lhx5 promotes forebrain development and activates transcription of secreted Wnt antagonists. *Development* **133**, 3191-3200.
Pera, E. M. and De Robertis, E. M. (2000). A direct screen for secreted proteins in Xenopus embryos identifies distinct activities for the Wnt antagonists Crescent and Frzb-1. *Mech. Dev.* **96**, 183-195.
Ploper, D., Lee, H. X. and De Robertis, E. M. (2011). Dorsal-ventral patterning: Crescent is a dorsally secreted Frizzled-related protein that competitively inhibits Tolloid proteases. *Dev. Biol.* **352**, 317-328.
Pokrywka, N. J. and Stephenson, E. C. (1991). Microtubules mediate the localization of bicoid RNA during Drosophila oogenesis. *Development* **113**, 55-66.
Pokrywka, N. J. and Stephenson, E. C. (1995). Microtubules are a general component of mRNA localization systems in Drosophila oocytes. *Dev. Biol.* **167**, 363-370.
Riechmann, V. and Ephrussi, A. (2001). Axis formation during Drosophila oogenesis. *Curr. Opin. Genet. Dev.* **11**, 374-383.
Rowning, B. A., Wells, J., Wu, M., Gerhart, J. C., Moon, R. T. and Larabell, C. A. (1997). Microtubule-mediated transport of organelles and localization of beta-catenin to the future dorsal side of Xenopus eggs. *Proc. Natl. Acad. Sci. USA* **94**, 1224-1229.
Schnorrer, F., Bohmann, K. and Nusslein-Volhard, C. (2000). The molecular motor dynein is involved in targeting swallow and bicoid RNA to the anterior pole of Drosophila oocytes. *Nat. Cell Biol.* **2**, 185-190.
Solnica-Krezel, L. and Driever, W. (1994). Microtubule arrays of the zebrafish yolk cell: organization and function during epiboly. *Development* **120**, 2443-2455.
Steinhauer, J. and Kalderon, D. (2006). Microtubule polarity and axis formation in the Drosophila oocyte. *Dev. Dyn.* **235**, 1455-1468.
Stepanova, T., Slemmer, J., Hoogenraad, C. C., Lansbergen, G., Dortland, B., De Zeeuw, C. I., Grosveld, F., van Cappellen, G., Akhmanova, A. and Galjart, N. (2003). Visualization of microtubule growth in cultured neurons via the use of EB3-GFP (end-binding protein 3-green fluorescent protein). *J. Neurosci.* **23**, 2655-2664.
Strahle, U. and Jesuthasan, S. (1993). Ultraviolet irradiation impairs epiboly in zebrafish embryos: evidence for a microtubule-dependent mechanism of epiboly. *Development* **119**, 909-919.
Streisinger, G., Walker, C., Dower, N., Knauber, D. and Singer, F. (1981). Production of clones of homozygous diploid zebra fish (Brachydanio rerio). *Nature* **291**, 293-296.
Takesono, A., Moger, J., Faroq, S., Cartwright, E., Dawid, I. B., Wilson, S. W. and Kudoh, T. (2012). Solute carrier family 3 member 2 (Slc3a2) controls yolk syncytial layer (YSL) formation by regulating microtubule networks in the zebrafish embryo. *Proc. Natl. Acad. Sci. USA* **109**, 3371-3376.
Tendeng, C. and Houart, C. (2006). Cloning and embryonic expression of five distinct sfrp genes in the zebrafish Danio rerio. *Gene Expr. Patterns* **6**, 761-771.
Topczewski, J. and Solnica-Krezel, L. (1999). Cytoskeletal dynamics of the zebrafish embryo. *Methods Cell Biol.* **59**, 205-226.
Vincent, J. P., Oster, G. F. and Gerhart, J. C. (1986). Kinematics of gray crescent formation in Xenopus eggs: the displacement of subcortical cytoplasm relative to the egg surface. *Dev. Biol.* **113**, 484-500.
Wagner, D. S., Dosch, R., Mintzer, K. A., Wiemelt, A. P. and Mullins, M. C. (2004). Maternal control of development at the midblastula transition and beyond: mutants from the zebrafish II. *Dev. Cell* **6**, 781-790.
Wang, S., Krinks, M., Lin, K., Luyten, F. P. and Moos, M., Jr (1997). Frzb, a secreted protein expressed in the Spemann organizer, binds and inhibits Wnt-8. *Cell* **88**, 757-766.
Weaver, C., Farr, G. H., 3rd, Pan, W., Rowning, B. A., Wang, J., Mao, J., Wu, D., Li, L., Larabell, C. A. and Kimelman, D. (2003). GBP binds kinesin light chain and translocates during cortical rotation in Xenopus eggs. *Development* **130**, 5425-5436.
Weil, T. T., Forrest, K. M. and Gavis, E. R. (2006). Localization of bicoid mRNA in late oocytes is maintained by continual active transport. *Dev. Cell* **11**, 251-262.
Westerfield, M. (2007). The Zebrafish Book. A Guide for the Laboratory Use of Zebrafish (Danio rerio), 5th Edition: University of Oregon Press.
Westfall, T. A., Hjertos, B. and Slusarski, D. C. (2003). Requirement for intracellular calcium modulation in zebrafish dorsal-ventral patterning. *Dev. Biol.* **259**, 380-391.
Wilkie, G. S. and Davis, I. (2001). Drosophila wingless and pair-rule transcripts localize apically by dynein-mediated transport of RNA particles. *Cell* **105**, 209-219.
Zimyanin, V. L., Belaya, K., Pecreaux, J., Gilchrist, M. J., Clark, A., Davis, I. and St Johnston, D. (2008). In vivo imaging of oskar mRNA transport reveals the mechanism of posterior localization. *Cell* **134**, 843-853.

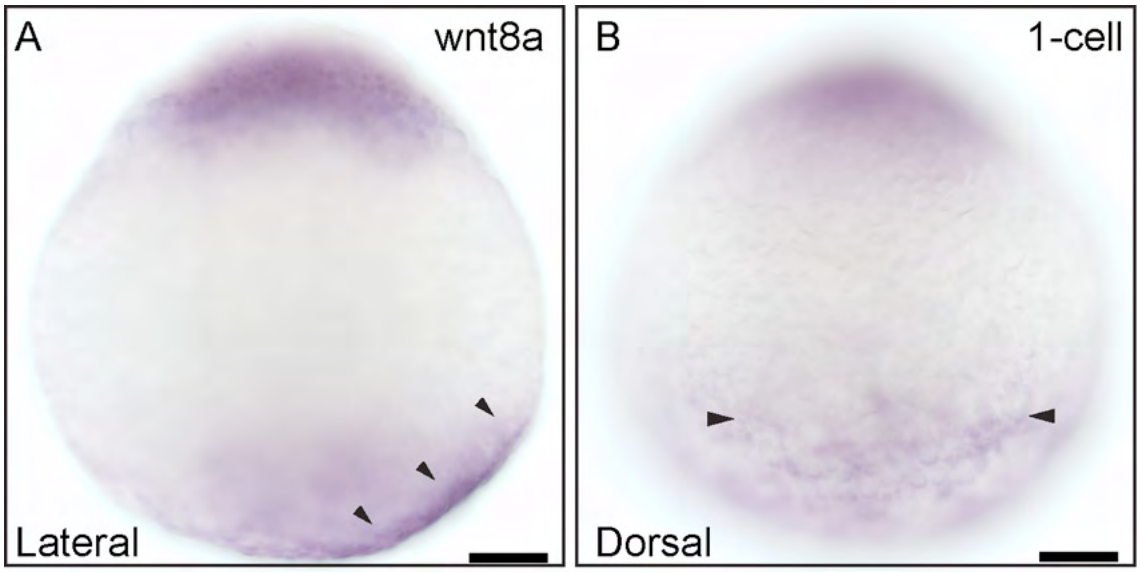

Fig. S1. Expression of maternal wnt8a in 1-cell stage embryos. (**A**) Lateral view showing asymmetric localization of *wnt8a* RNA on the vegetal cortex (arrowheads). (**B**) Dorsal view showing the extent of *wnt8a* RNA distribution on the yolk cortex (arrowheads), along the animal-vegetal axis. Scale bars: 50 μm.

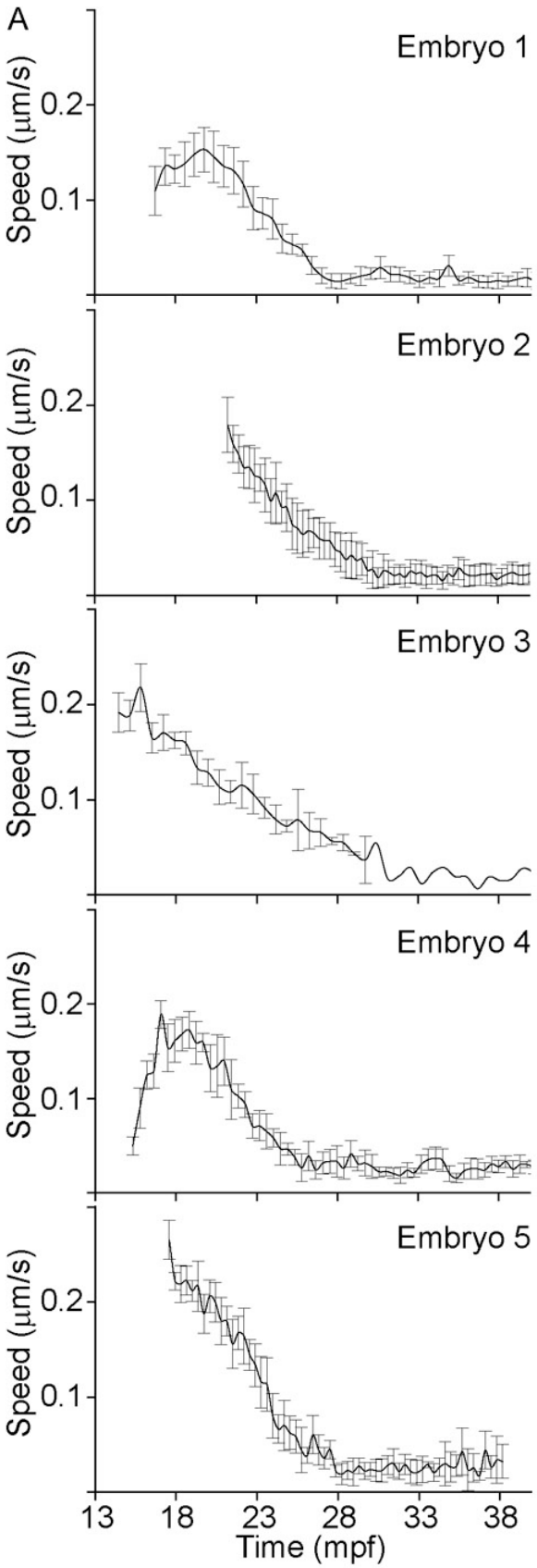

Fig. S2. Speed of cytoplasmic granules (μm/second) along parallel arrays in individual embryos. Graph shows rapid early movement, and slowing down of granules after 30 mpf, when parallel arrays disappear. Error bars are shown for all time points and represent s.d. *n*=11 granules for embryo 1; *n*=16 granules for embryo 2; *n*=4 granules for embryo 3; *n*=6 granules for embryo 4; *n*=8 granules for embryo 5.

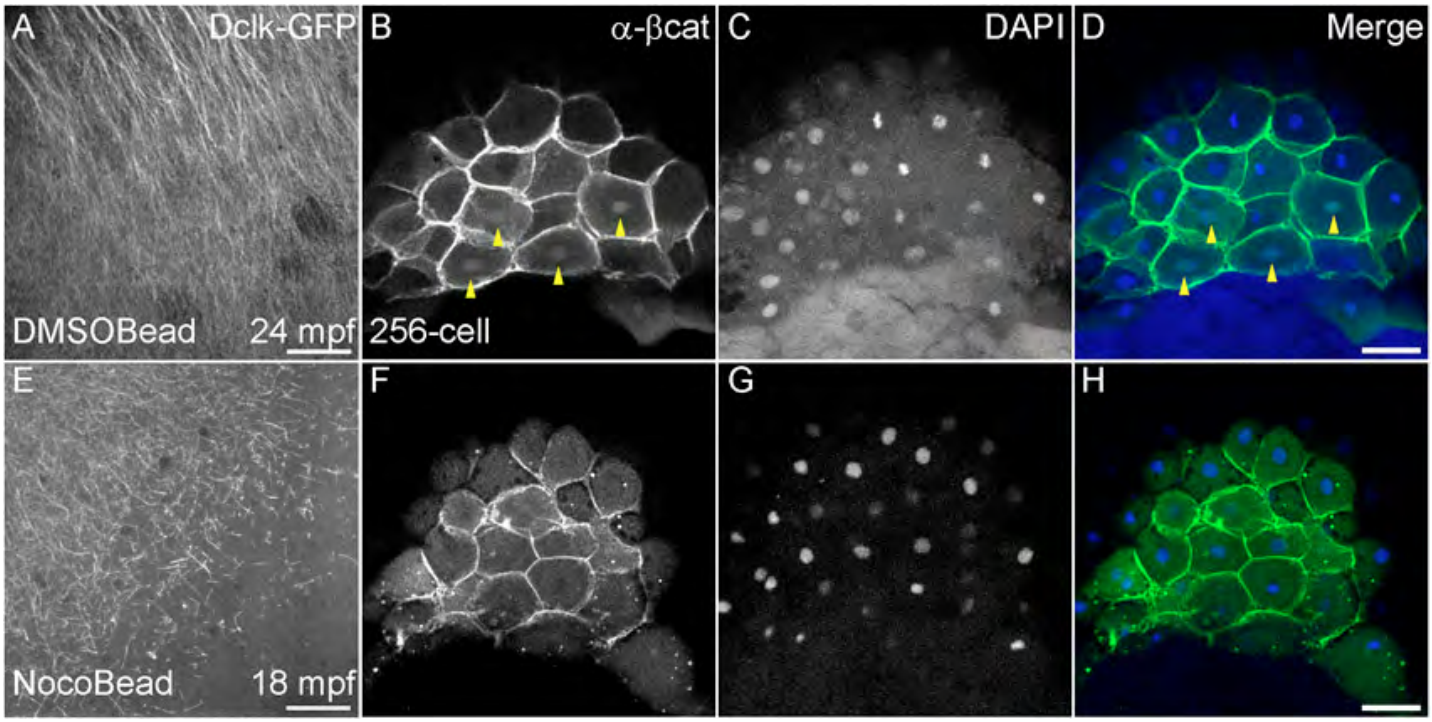

Fig. S3. Transient and local disruption of parallel microtubule arrays affects dorsal specification. (**A**,**E**) Dcklk-GFP labeled arrays shows local disruption in nocodazole bead-treated embryos (E) in comparison with control DMSO bead-treated embryos (A). (**B**,**F**) Nuclear accumulation of β-Catenin in DMSO bead-treated embryos (yellow arrowheads in B), in comparison with absence of β-Catenin in nocodazole bead-treated embryos (F). (**C**,**D**,**G**,**H**) DAPI staining (C,G) shows all nuclei in control and nocodazole-treated embryos, and D,H show merged images for β-Catenin and DAPI staining. Scale bars: in A,E, 30 μm; in D,H, 50 μm.

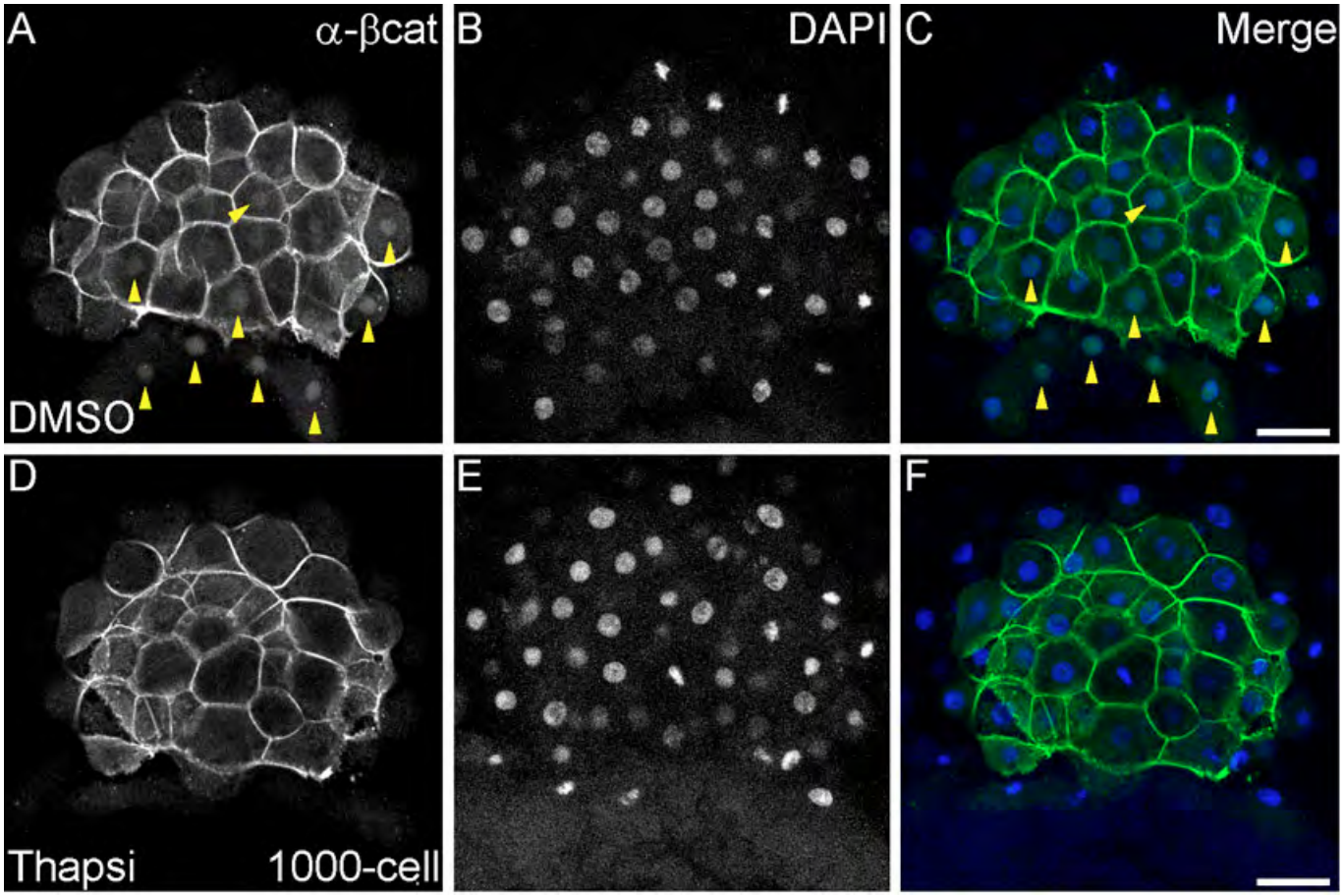

Fig. S4. Disruption of Ca^{2+} signaling affects dorsal specification. (**A**,**D**) Dorsal nuclear accumulation β-Catenin in DMSO-treated embryos (yellow arrowheads in A) in comparison with absence of β-Catenin in thapsigargin-treated embryos (D). (**B**,**C**,**E**,**F**) DAPI staining (B,E) shows all nuclei in control and thapsigargin-treated embryos, and C,F show merged images for β-Catenin and DAPI staining. Scale bars: 50 μm.